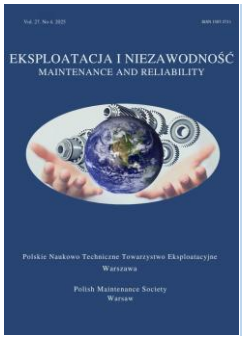

Eksploatacja i Niezawodnosc – Maintenance and Reliability
Volume 27 (2025), Issue 4
journal homepage: http://www.ein.org.pl

Article citation info:
Luo X, Bu W, Liang H, Zheng M, Convolutional Neural Network - Gated Recurrent Unit combined with Error Correction for Lithium Battery State of Health Estimation, Eksploatacja i Niezawodnosc – Maintenance and Reliability 2025: 27(4) http://doi.org/10.17531/ein/202184

Convolutional Neural Network - Gated Recurrent Unit combined with Error Correction for Lithium Battery State of Health Estimation

Indexed by: Web of Science Group

Xing Luo[a], Wenxie Bu[a], Han Liang[a], Minggang Zheng[a,*]

[a] School of Mechanical Engineering, Shandong Jianzhu University, China

Highlights

- HFs are extracted from partial charging data to enhance practical applicability.
- A CNN-GRU hybrid model is developed for precise SOH estimation of lithium-ion batteries.
- GPR-MC is employed to dynamically correct errors and optimize estimation accuracy.

Abstract

To accurately estimate the State of Health (SOH) of lithium-ion batteries, this study proposes a novel approach combining a Convolutional Neural Network (CNN) and a Gated Recurrent Unit (GRU) with an error correction mechanism. By extracting health features from partial charging data, this method reduces dependence on complete charge-discharge cycles, addressing challenges like long data acquisition times and high costs. The CNN captures local features of battery degradation, while the GRU models aging dynamics to provide an initial SOH estimate. An error correction strategy using Gaussian Process Regression (GPR) and Markov Chain (MC) further refines the results. GPR models nonlinear relationships to optimize predictions, and MC adjusts error distributions dynamically. Experiments on the University of Maryland dataset demonstrate that this method achieves lower Root Mean Square Error (RMSE) and Mean Absolute Error (MAE) than benchmark techniques, proving its accuracy and robustness.

Keywords
lithium-ion battery, state of health, CNN, GRU, error correction

1. Introduction

Lithium-ion batteries, recognized for their long lifespan and high energy efficiency, have become increasingly popular in electric vehicles and energy storage systems [1]. Within Battery Management Systems (BMS), accurately determining the State of Health (SOH) of lithium-ion batteries is essential. Reliable SOH estimation not only ensures batteries operate safely and stably but also prolongs their lifespan and enables timely maintenance recommendations for users. However, as batteries age and are subjected to prolonged use, performance inevitably deteriorates. Consequently, the development of a highly precise SOH estimation model has emerged as a significant challenge in battery management research [2].

The SOH is defined as the ratio of a battery's current maximum available capacity to its rated capacity [3], expressed as follows:

$$SOH = \frac{Q_{\mathrm{cu}}}{Q_{\mathrm{e}}} \times 100\% \quad (1)$$

where Q_{cu} represents the current maximum available capacity, and Q_{e} denotes the rated capacity.

Battery SOH estimation methods are typically divided into

(*) Corresponding author.
E-mail addresses: X. Luo (ORCID: 0009-0001-1304-565X) 19861801070@163.com, W. Bu (ORCID: 0009-0002-5734-6937) 18615663880@163.com, H. Liang (ORCID: 0009-0009-6085-1054) lianghan202411@163.com, M. Zheng (ORCID: 0000-0002-4235-403X) 12665@sdjzu.edu.cn

two main categories: model-based approaches and data-driven approaches [4]. Model-based methods rely heavily on constructing equivalent circuit models to determine SOH. For instance, Bustos et al. [5] proposed a methodology integrating the Kalman Filter (KF) with an innovative Sliding Innovation Filter (SIF). Ranga et al. [6] introduced a novel technique employing the Unscented Kalman Filter (UKF), while Ling et al. [7] developed an approach utilizing the Dual Fractional-Order Extended Kalman Filter (DEKF). Furthermore, Xiong et al. [8] put forward a strategy combining Dual Adaptive Extended Kalman Filtering (DAEKF) for SOH estimation.

Although these model-based methods leverage battery physical characteristics for accurate predictions, they often demand extensive electrochemical expertise and highly precise parameter inputs. This makes their application challenging in real-world scenarios, where obtaining such parameters is difficult and time-intensive [9].

In contrast to model-based approaches, data-driven SOH estimation methods have gained significant attention in recent years, primarily due to their ability to predict SOH directly by extracting features from operational battery data and applying machine learning or deep learning techniques [10]. For instance, Zhi et al. [11] proposed a hybrid method that combines Genetic Algorithm-Particle Swarm Optimization (GA-PSO) to optimize the parameters of a Support Vector Regression (SVR) model, subsequently applying it for SOH estimation. Similarly, Dai et al. [12] identified initial health features (HFs) derived from battery parameters such as voltage, current, temperature, Incremental Capacity (IC) curves, and Differential Thermal Voltage (DTV) curves, and utilized a dual-kernel Gaussian Process Regression (NGO-GPR) model for SOH estimation. Wu et al. [13] introduced a lithium-ion battery SOH prediction framework integrating Variational Mode Decomposition (VMD) with a Dung Beetle Optimization-Support Vector Regression (DBO-SVR) model. In another study, Wu et al. [14] proposed a method that combines HF extraction from charging voltage curves with Ridge Regression (RR) to estimate SOH and predict Remaining Useful Life (RUL). Additionally, Wang et al. [15] concentrated on extracting three specific HFs from battery charge-discharge cycles, including time intervals corresponding to identical charging and discharging voltage levels and the time related to internal temperature variations during discharge, employing an enhanced GPR model to estimate SOH.

In recent years, deep learning techniques have seen extensive application in SOH estimation tasks. Particularly, hybrid neural network architectures have emerged as a focal area of research due to their capability to combine the strengths of different models, significantly enhancing predictive accuracy. For instance, Liao et al. [17] leveraged incremental capacity (IC) curves from battery discharge data and applied Gaussian filtering for noise reduction. They proposed a hybrid framework incorporating a Convolutional Neural Network (CNN) and a Multi-Layer Perceptron (MLP) to estimate the SOH of lithium-ion batteries. Wang et al. [18] extracted 19 critical features from charging voltage, current, temperature, and IC curves and utilized a model optimized by Particle Swarm Optimization (PSO) and a Generalized Regression Neural Network (GRNN) for prediction. Geng et al. [19] proposed a method that combines energy indicators from voltage and temperature signals with other metrics like capacity intervals, using a Back Propagation (BP) neural network optimized via a genetic algorithm for SOH prediction. Xu et al. [20] introduced a CNN-LSTM model enhanced by skip connections, which employs IC curves for SOH estimation. Lin et al. [21] identified health indicators from IC, differential thermal voltage (DTV), and other curves, employing an LSTM with attention mechanisms for SOH assessment. Park et al. [22] utilized multi-channel features like voltage, current, and temperature data for SOH estimation, relying on LSTM networks for accuracy. Dai et al. [23] employed features like average voltage and capacity increments within a Prior Knowledge Neural Network (PKNN) framework enhanced by a Markov Chain for improved predictions.Ping et al. [24] utilized discharge sequence data from retired batteries, deploying a modified LSTNet model for SOH estimation. Li et al. [25] selected health features including charging voltage and curve statistics to estimate SOH and SOC in retired batteries using an AdaBoost.Rt-LSTM ensemble learning algorithm. Wang et al. [26] proposed a hybrid model leveraging Multi-Feature Extraction (MFE), GRU, and Temporal Convolutional Attention (TCA) mechanisms to predict SOH and RUL. Nasimov et al. [27] integrated improved Particle Swarm Optimization (IPSO) with BiLSTM for health estimation based on charge-discharge cycle data. Li et al. [28] introduced a Temporal Convolutional Network-Long Short-

Term Memory (TCN-LSTM) hybrid model for SOH and RUL estimation, while Song et al. [29] used XGBoost with a focus on multi-feature correction. Zhao et al. [30] proposed a Bayesian regularized neural network combined with a KNN-Markov strategy for SOH improvement. Wei et al. [31] focused on retired batteries, extracting parameters like Urest, TDCH, and ICpeak for use in a neural network integrated with a Markov Chain for SOH evaluation. Zou et al. [32] explored equal interval discharge time and IC analysis within a BiLSTM model with Attention Mechanisms (AM) for SOH prediction. Recent studies, including [23, 29, 30, 31], have emphasized error correction methodologies, which significantly improve prediction precision and reliability by refining initial estimations.

In data-driven SOH estimation methods, the extraction of health features (HFs) is crucial. However, due to limitations in sensor deployment, obtaining battery temperature data often poses significant challenges [33]. Additionally, compared to the discharge process, data acquisition during the charging process is more feasible, but the charging process may not always start from a fully discharged state or reach full capacity. To address this issue, this study proposes a method for extracting health features from partial charging data, thereby effectively reducing reliance on complete charge-discharge data.

The degradation of battery SOH is a complex process characterized by significant temporal dynamics. To more accurately capture the dynamic changes in battery SOH, this study employs a Gated Recurrent Unit (GRU) model from the Recurrent Neural Network (RNN) family, combined with the feature extraction capabilities of a Convolutional Neural Network (CNN). CNNs can extract local spatial features from the battery aging process, while GRUs capture long-term dependencies in the temporal characteristics of battery aging. Previous studies [17][20] have demonstrated the excellent performance of similar hybrid models in SOH estimation. The combination of CNN and GRU allows the model to effectively integrate spatial and temporal features. Compared to other hybrid networks such as CNN-LSTM or BiLSTM, CNN-GRU offers greater simplicity, making it better suited for large-scale data scenarios and dynamic application environments in lithium battery SOH prediction.

Although CNN-GRU provides relatively accurate preliminary predictions, the results may still be affected by data noise and complex nonlinear relationships, leading to systemic bias or local errors. To further improve prediction accuracy, this study introduces an error correction strategy based on Gaussian Process Regression (GPR) and Markov Chain (MC). GPR, as a nonparametric regression method grounded in Bayesian theory, captures the complex nonlinear relationships between prediction errors and input features while quantifying the uncertainty of predictions. MC dynamically models the evolution of error distributions through state transition matrices, making it particularly well-suited for describing the temporal dynamics of error sequences. The combination of GPR and MC not only corrects systemic biases in preliminary predictions but also dynamically adjusts the error model to accommodate complex distributions in different states. Similar strategies have been shown in other studies [29][30] to significantly improve SOH prediction accuracy, particularly in scenarios with high noise levels or complex data distributions.

The paper is structured as follows: Section 2 provides a detailed description of the dataset, the extracted health features, and correlation analysis; Section 3 delves into the theoretical foundations and the structure of the proposed model; Section 4 presents algorithm validation, results, and analysis; and Section 5 summarizes the conclusions of the study.

2. Dataset Description and Health Feature Extraction

2.1. Dataset Description

This research employs the University of Maryland's battery aging dataset as the source of experimental data, focusing on three specific batteries: CS35, CS36, and CS37. The dataset provides comprehensive information on the batteries' charging and discharging behavior. These batteries are LiCoO2 lithium-ion types with a nominal capacity of 1.1 Ah. Measurements were conducted using an Arbin battery testing system, following a Constant Current (CC) - Constant Voltage (CV) charging methodology and executing discharge tests under a constant current protocol.

2.2. Health Feature Extraction

Figure 1 shows the voltage curves of the three batteries at different cycle intervals. As the number of cycles increases, the aging of the batteries becomes progressively more severe,

characterized by a gradual reduction in charging time.

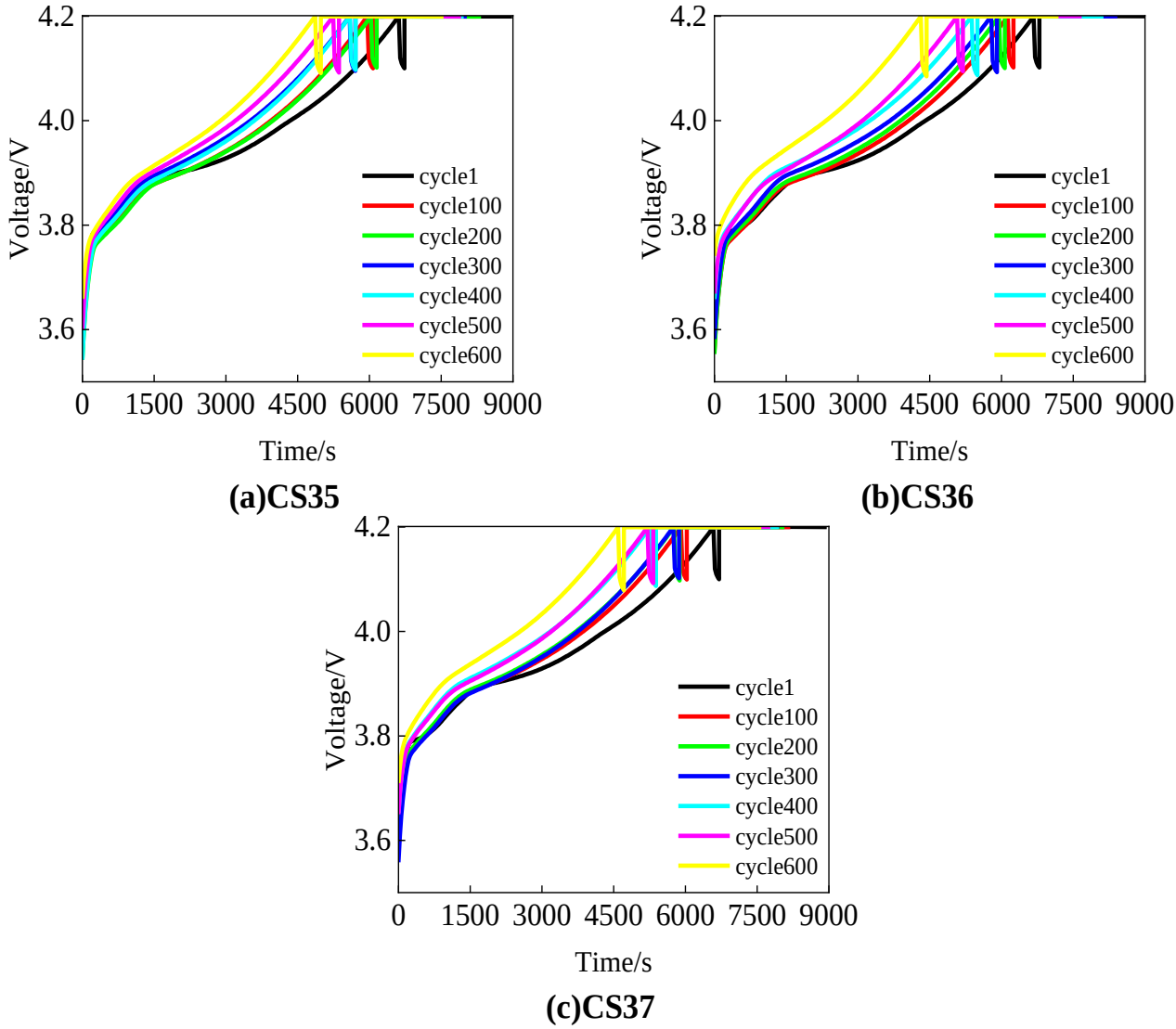

Figure 1. Voltage curves under different cycles.

To better align with practical application scenarios, this study considers that batteries in actual usage may not always start charging from the cutoff discharge voltage or reach full charge. Therefore, the following five HFs were extracted:

HF1: The constant current charging time within the voltage range of 3.75V to 4.15V, representing the time required for the battery to charge within this specific range.

HF2: The integral of the voltage-time curve within the same voltage range, reflecting the cumulative charging behavior of the battery in this interval.

HF3: The average voltage within the 3.75V to 4.15V range, serving as an indicator of the overall voltage level of the battery in this interval and indirectly reflecting the battery's capacity change trend.

HF4: The maximum rate of voltage change (maximum voltage change rate), which characterizes the dynamic response of the battery during the charging process. Its fluctuation amplitude can indirectly reflect the degree of battery aging.

HF5: The ratio of the standard deviation to the mean of voltage changes (voltage variation coefficient), used to measure the relative extent of voltage fluctuations.

2.3. Correlation Analysis

To evaluate the relationship between HFs and SOH, this research utilizes both the Pearson correlation coefficient and the Spearman correlation coefficient. Their mathematical representations are provided below as equations (2) and (3), respectively:

$$Pearson = \frac{E(XY) - E(X)E(Y)}{\sqrt{E(X^2) - E^2(X)}\sqrt{E(Y^2) - E^2(Y)}} \quad (2)$$

$$Spearman = \frac{\sum_{i=1}^{n}(X_i - \bar{X})(Y_i - \bar{Y})}{\sqrt{\sum_{i=1}^{n}(X_i - \bar{X})^2}\sqrt{\sum_{i=1}^{n}(Y_i - \bar{Y})^2}} \quad (3)$$

Table 1. Correlation Coefficient Analysis.

HF	Correlation Coefficient	CS35	CS36	CS37
HF1	Pearson	99.7400	99.8313	99.7681
	Spearman	99.6314	99.8359	99.6496
HF2	Pearson	99.7617	99.8466	99.7860
	Spearman	99.6518	99.8370	99.6552
HF3	Pearson	-96.9381	-96.6624	-96.5870
	Spearman	-95.8434	-96.6787	-95.6690
HF4	Pearson	-88.5515	-84.2194	-86.1015
	Spearman	-86.1785	-85.2394	-86.9546
HF5	Pearson	89.3308	87.0211	86.1560
	Spearman	85.1085	88.6657	86.1658

Table 1 shows that the correlation coefficients of HF1 and HF2 exceed 99%, indicating a very strong positive correlation with SOH. This suggests that constant-current charging time and charging integral are key features for evaluating battery health status. In contrast, although HF3 and HF4 exhibit negative correlations with SOH and HF5 shows a positive correlation, the correlations of these three health features with SOH are significantly lower than those of HF1 and HF2. Therefore, this study ultimately selects HF1 and HF2 as input features.

Figure 2 illustrates the degradation trends of SOH, HF1, and HF2 of battery CS35 with the increase in cycle count. The results show that both HF1 and HF2 exhibit significant attenuation as the cycle count increases, which is highly consistent with the degradation trend of SOH. This consistency indicates that the selected health features effectively reflect the aging state of the battery. By adopting this feature extraction method, the health features used in this study reduce reliance on full lifecycle data, simplify data collection, and enhance the model's applicability in practical scenarios.

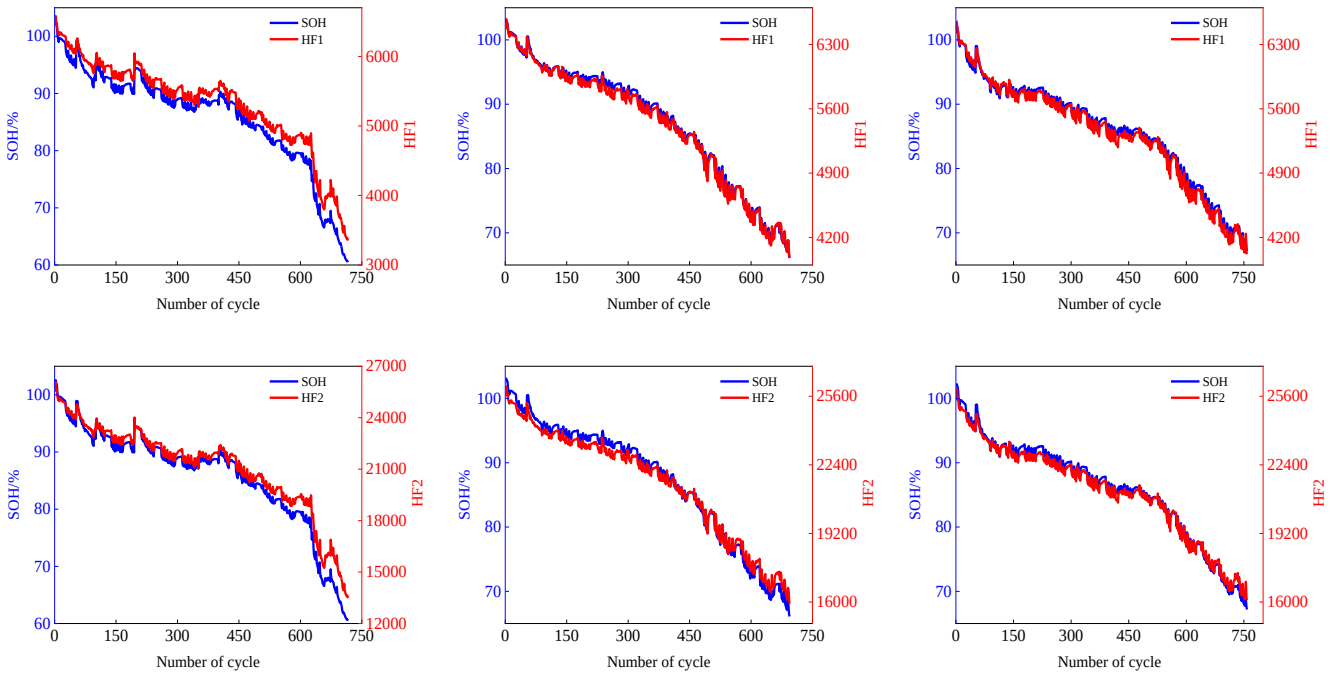

Figure 2. Degradation trends of health features and SOH with cycle count.

3. SOH Estimation Method

This paper proposes an SOH estimation method based on a CNN-GRU model combined with a GPR-MC error correction strategy. The method leverages the capability of CNN to extract sequential features in the time dimension, the ability of GRU to dynamically learn temporal data, and the statistical advantages of GPR-MC in error correction. First, the CNN-GRU model is used to perform an initial SOH estimation, followed by GPR-MC for error correction. The estimation process is shown in Figure 3.

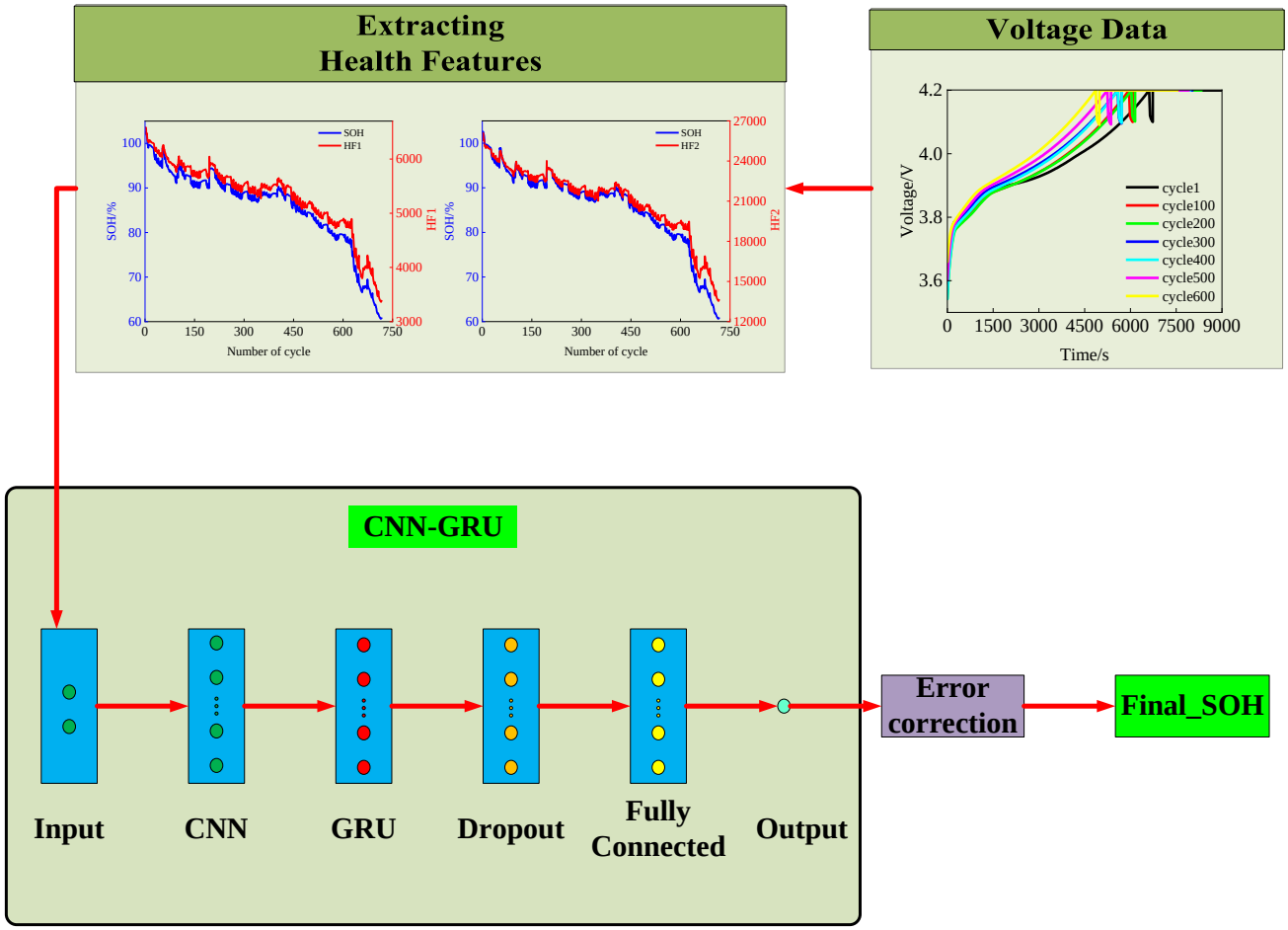

Figure 3. SOH Estimation Model.

3.1. Initial SOH Estimation

1.CNN

A CNN is a type of feedforward neural network extensively applied in tasks like feature extraction and pattern recognition [34]. By performing convolution operations, CNNs extract features from input data, progressively building higher-level feature representations through layered processing. These features are eventually processed by fully connected layers to achieve tasks such as classification or regression.

The conventional structure of a CNN includes the following components: input layer, convolutional layers, pooling layers, fully connected layers, and output layer. Convolutional layers apply sliding window filters to input data to generate feature maps. Pooling layers are used to downsample these feature maps, thereby preserving essential information while reducing computational complexity. Fully connected layers combine the features from earlier layers to generate the final output. For sequential data applications, such as battery state of health estimation, one-dimensional CNNs (1D CNNs) offer significant advantages.

The mathematical representation of the convolutional layer's output can be expressed as:

$$h_{cnn} = \sigma(\omega_{cnn} \times x_t + b_{cnn}) \quad (4)$$

where ω_{cnn} denotes the weight, b_{cnn} represents the bias, σ is the activation function, and x_t is the input data at a given time step.

2.GRU

The GRU, an improved version of the RNN [25], addresses the common issue of gradient vanishing when handling long sequential data. As illustrated in Figure 4, it introduces two key gating mechanisms—update and reset gates—that control the information flow. These gates help the GRU effectively determine which data should be retained or discarded, enhancing its ability to capture long-term dependencies within sequential data. This architecture not only strengthens the GRU's capacity to model temporal relationships but also reduces the number of parameters, thereby increasing computational efficiency.

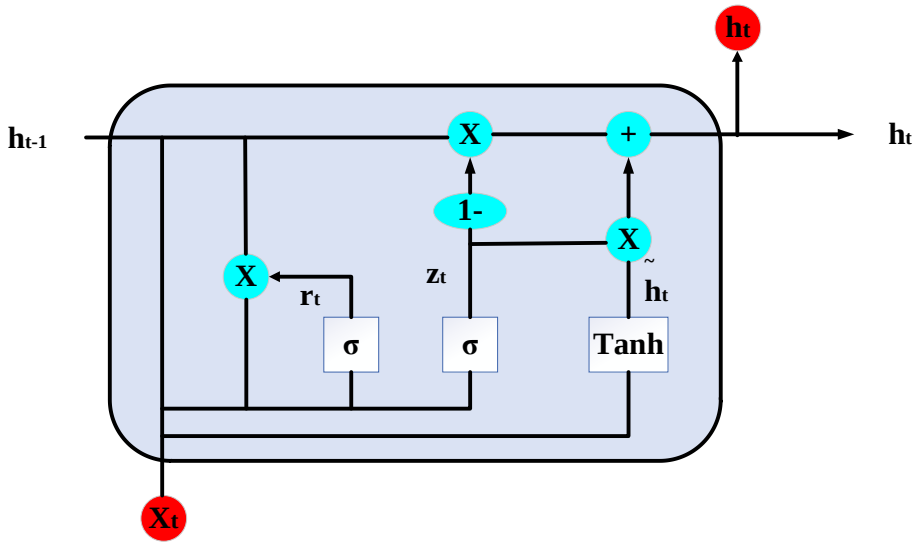

Figure 4. GRU Structure Diagram.

The GRU operates based on two primary gates:

Update Gate: This gate regulates the extent to which information from the previous hidden state is carried forward to the current state, enabling efficient transfer of information across time steps.

Reset Gate: This gate manages the influence of the previous hidden state on the current input, allowing the model to selectively ignore unnecessary historical information for better adaptation to new inputs.

The computational process of GRU is described mathematically as follows:

$$z_t = \sigma(W_z \cdot [h_{t-1}, x_t]) \quad (5)$$

$$r_t = \sigma(W_r \cdot [h_{t-1}, x_t]) \quad (6)$$

$$\tilde{h}_t = tanh(W \cdot [r_t * h_{t-1}, x_t]) \quad (7)$$

$$h_t = (1 - z_t) * h_{t-1} + z_t * \tilde{h}_t \quad (8)$$

where, x_t signifies the current input, h_{t-1} denotes the previous hidden state, and h_t represents the hidden state passed to the next time step. $\tilde{h}_t$ is the candidate hidden state, while r_t and z_t correspond to the reset and update gates, respectively.

The CNN-GRU framework in this study is designed with two inputs and one output. The Adam optimization algorithm is utilized, initialized with a learning rate of 0.01, a maximum of 1000 iterations, and a dropout rate of 0.1. For the CNN component, the convolutional kernel size is set to 10, with 64 kernels employed. Details of GRU parameter exploration and optimization are elaborated in Section 4.2.

3.2. Error Correction

GPR is a regression method based on a non-parametric Bayesian framework. Its theoretical foundation lies in modeling the nonlinear relationship between input features and output targets through kernel functions. In error correction, GPR uses the predicted value as the input feature and the initial prediction error as the output target. By employing a Gaussian radial basis function (RBF) kernel, it learns the distribution pattern between the input and error, allowing precise modeling of the error. GPR has the following characteristics: it can capture complex nonlinear error distributions and provide both the predicted mean and its uncertainty, facilitating subsequent processing.

MC utilizes a state transition probability matrix to describe the dynamic changes in the error distribution. Its theoretical foundation lies in the time-series characteristics of the Markov process, where the current state depends only on the previous state. In error correction, MC constructs state divisions and transition matrices to dynamically adjust the error distribution, with the following advantages: it allows dynamic adaptation of error distribution to different sample states and enables flexible adjustments between different states, improving the robustness and accuracy of the correction results.

This paper proposes a dynamic error correction method by modeling the error using training data and combining GPR with MC. The specific process is as follows:

First, the initial prediction error is calculated based on the training data. The Gaussian Process Regression model is used to model the error, with the predicted value as the input feature and the error as the output target, resulting in an error adjustment model. The GPR model uses a Gaussian radial basis function (RBF) kernel, and its parameters are optimized by

maximizing the marginal likelihood.

The error is normalized to the range [0,1] to facilitate subsequent state division and processing. The normalized error is divided into three states based on its mean μ and standard deviation σ：

State1: [0, μ−0.5)

State2: [μ−0.5, μ+0.5σ)

State3: [μ+0.5σ, 1]

Data is assigned to the corresponding state based on the value of the normalized error, describing the characteristics of the error distribution. Based on the sequence of error states, the transition frequencies between states are calculated to construct a state transition matrix P. For each state, the average value of the correction error is computed to form a state error matrix Q.

During the testing phase, the test error adjustment values are obtained based on the initial estimates. These adjustment values are normalized and assigned to the corresponding state based on the defined state intervals. Using the state sequence of the test data, along with the state transition matrix P and state error matrix Q, the test error is dynamically corrected to produce the final estimation result.

4. Experiments and Analysis

This research carried out three simulation experiments using the battery aging dataset from the University of Maryland. The experiments focused on data from three specific batteries: CS35, CS36, and CS37. The model's performance was assessed through the Leave-One-Out Cross-Validation approach, where in each iteration, one battery's data was designated as the test set, and the remaining two batteries' data were utilized as the training set.

4.1. Evaluation Metrics

To assess the model's predictive performance, this study utilizes two widely recognized error metrics: Root Mean Square Error (RMSE) and Mean Absolute Error (MAE). These metrics provide a quantitative approach to analyze the model's prediction accuracy. The formulas are defined as follows:

$$RMSE = \sqrt{\frac{1}{n}\sum_{i=1}^{n}(\hat{y}_i - y_i)^2} \tag{9}$$

$$MAE = \frac{1}{n}\sum_{i=1}^{n}|\hat{y}_i - y_i| \tag{10}$$

In these equations, $\hat{y}_i$ represents the predicted value for the i-th data point, y_i is the corresponding actual value, and n denotes the total number of predictions.

4.2. Determining CNN-GRU Model Parameters

GRU plays a pivotal role in SOH estimation. This section examines the impact of GRU layers and the number of neurons in the network. The neuron counts are set at 32, 64, and 128, while the GRU layer counts are configured to 1, 2, and 3. Using CS35 as a case study, the hyperparameters of the GRU network are analyzed. Initially, the GRU layer count is fixed at 1, and the SOH estimation performance for neuron counts of 32, 64, and 128 is assessed.

Table 2 presents the estimation errors for different neuron configurations. When neurons are set to 32, the RMSE and MAE are 0.7046% and 0.5378%, respectively. For 64 neurons, the RMSE decreases to 0.5661%, and MAE reduces to 0.4382%. With 128 neurons, the RMSE is 0.6043%, and MAE is 0.4525%. When the number of GRU neurons is set to 64, the model achieves lower RMSE and MAE compared to other settings, indicating that an appropriate number of neurons can achieve the optimal balance between complexity and generalization ability.

Table 2. Estimation errors under different neuron counts.

Number	RMSE (%)	MAE (%)
32	0.7046	0.5378
64	**0.5661**	**0.4382**
128	0.6043	0.4525

Figure 5 depicts the SOH estimation outcomes and associated errors for three distinct neuron counts. By cross-referencing Table 2 and Figure 5, it becomes evident that the estimation accuracy is the lowest when the neuron count is set at 32, reaches its highest at 64 neurons, and is marginally reduced at 128 neurons, though the difference between 64 and 128 is minimal. To further explore the impact of network layers, the number of hidden layer neurons is fixed at 64, and the influence of GRU layers on SOH estimation performance is investigated.

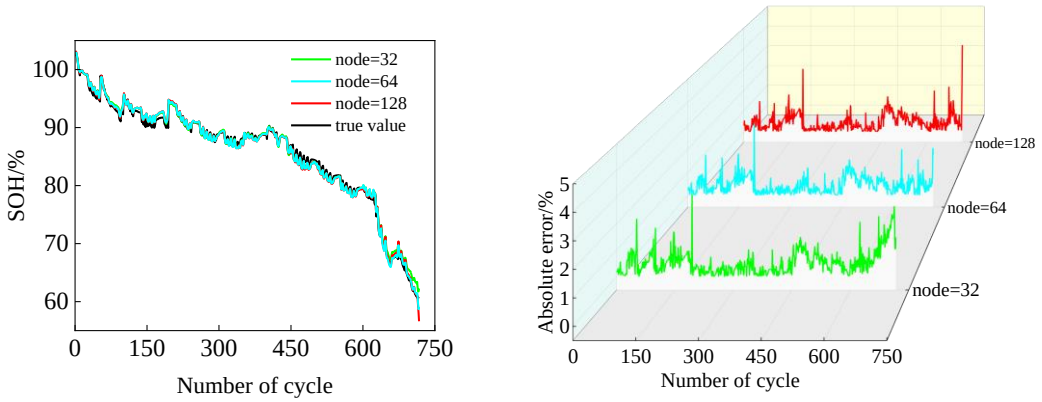

Figure 5. SOH estimation results and errors under different neuron counts.

Table 3 presents the SOH estimation accuracy for three different layer numbers when the number of neurons is set to 64. Figure 6 illustrates the SOH estimation results and errors under different layer numbers. As shown in Table 3, when the number of layers is 1 and the number of neurons is 64, the RMSE is 0.5661% and the MAE is 0.4382%, achieving the highest estimation accuracy. Increasing the number of layers does not improve estimation accuracy and may introduce risks of overfitting and increased computational costs. Therefore, this study ultimately determines that the optimal GRU configuration is 64 neurons and 1 layer.

Table 3. Estimation errors under different layer numbers.

Number	RMSE (%)	MAE (%)
1	**0.5661**	**0.4382**
2	0.5788	0.4404
3	0.7098	0.5185

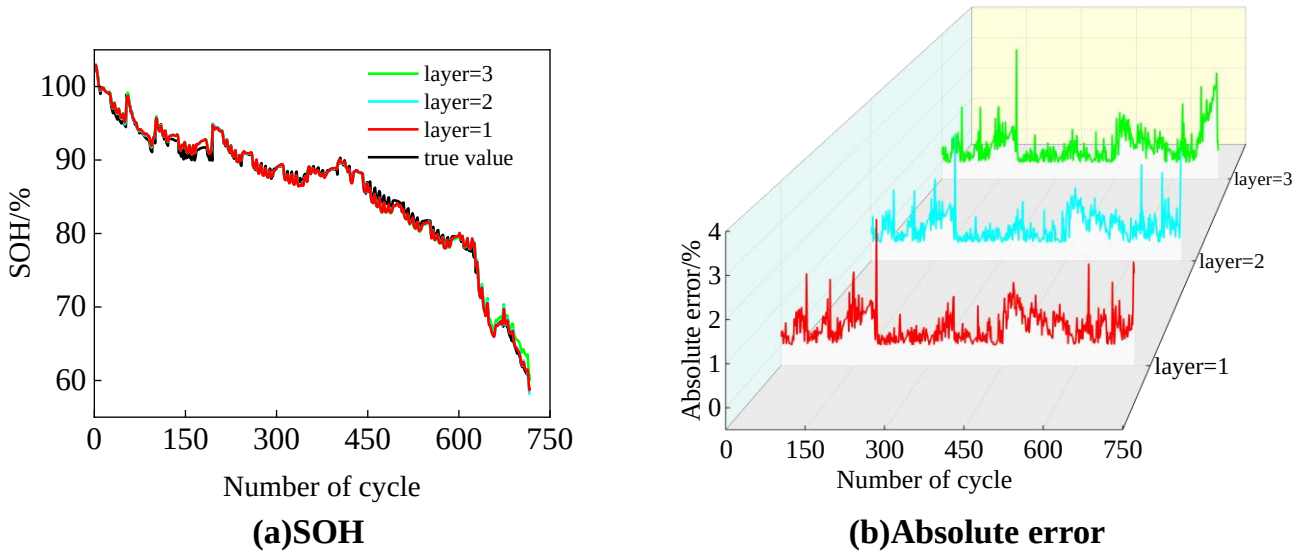

Figure 6. SOH estimation results and errors under different layer numbers.

Table 4. Estimation errors of the CNN-GRU model.

Battery	RMSE (%)	MAE (%)
CS35	0.5661	0.4382
CS36	0.6937	0.6083
CS37	0.4424	0.3500
Average	0.5674	0.4655

Table 4 and Figure 7 present the SOH estimation results and errors of the finalized model. As shown in Table 4, the model achieves the highest estimation accuracy on the CS37 battery, with RMSE = 0.4424% and MAE = 0.3500%. The estimation accuracy is the lowest on the CS36 battery, with RMSE = 0.6937% and MAE = 0.6083%.

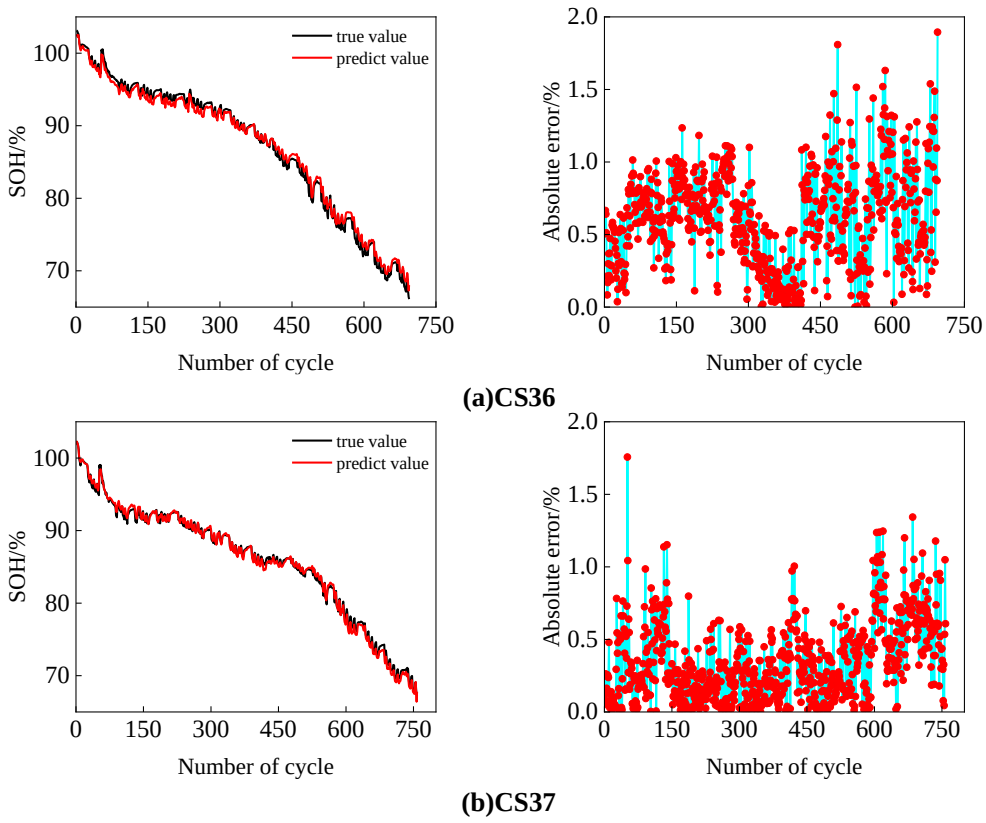

Figure 7. SOH estimation results and errors.

4.3. Comparative Analysis with Other Algorithms

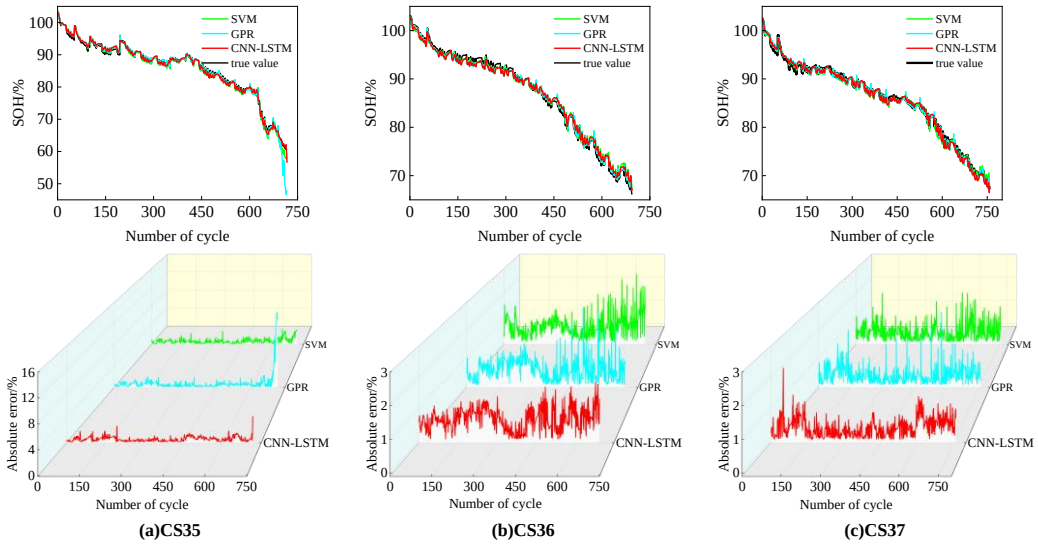

Figure 8. SOH estimation results and errors of SVM, GPR, and CNN-LSTM.

This subsection introduces a comparative analysis involving SVM, GPR, and CNN-LSTM models. Table 5 presents the estimation errors of the three models across three batteries, while Figure 8 illustrates the SOH estimation results and absolute errors for each model. As shown in Tables 4 and 5, the proposed CNN-GRU achieves an RMSE of 0.5674% and an MAE of 0.4655%, which outperforms the SVM model (average RMSE = 0.6872%, average MAE = 0.5380%) and the GPR model (average RMSE = 0.9558%, average MAE = 0.5381%). This improvement in estimation accuracy is mainly attributed to the local feature extraction capability of CNN and the strength of GRU in handling long-sequence data. Furthermore,

compared to the more complex CNN-LSTM model (average RMSE = 0.6216%, average MAE = 0.5125%), CNN-GRU maintains higher accuracy while simplifying the network structure.

Table 5. Estimation errors of the comparative models.

Method	Battery	RMSE (%)	MAE (%)
SVM	35	0.8001	0.5903
	36	0.7570	0.6357
	37	0.5055	0.3879
	Average	0.6872	0.5380
GPR	35	1.7192	0.7040
	36	0.6741	0.5516
	37	0.4740	0.3589
	Average	0.9558	0.5381
CNN-LSTM	35	0.6378	0.4970
	36	0.7421	0.6533
	37	0.4850	0.3872
	Average	0.6216	0.5125

4.4. Results After Error Correction

Table 6 highlights the SOH estimation errors for the three batteries following the application of error correction. As indicated, the RMSE and MAE values for CS35 are 0.2154% and 0.1746%, respectively. For CS36, the RMSE is 0.2514% while the MAE stands at 0.2313%. Similarly, for CS37, the RMSE and MAE are recorded as 0.3128% and 0.2652%, respectively. Figure 9 provides a visual representation using CS37 as an example, showing the SOH estimation results and corresponding absolute errors post error correction. When comparing these findings with Table 4 and Figure 7, it becomes apparent that the SOH estimation accuracy has been significantly enhanced through the error correction process.

Table 6. Estimation errors after error correction.

Battery	RMSE (%)	MAE (%)
CS35	0.2154	0.1746
CS36	0.2514	0.2313
CS37	0.3128	0.2652
Average	0.2599	0.2237

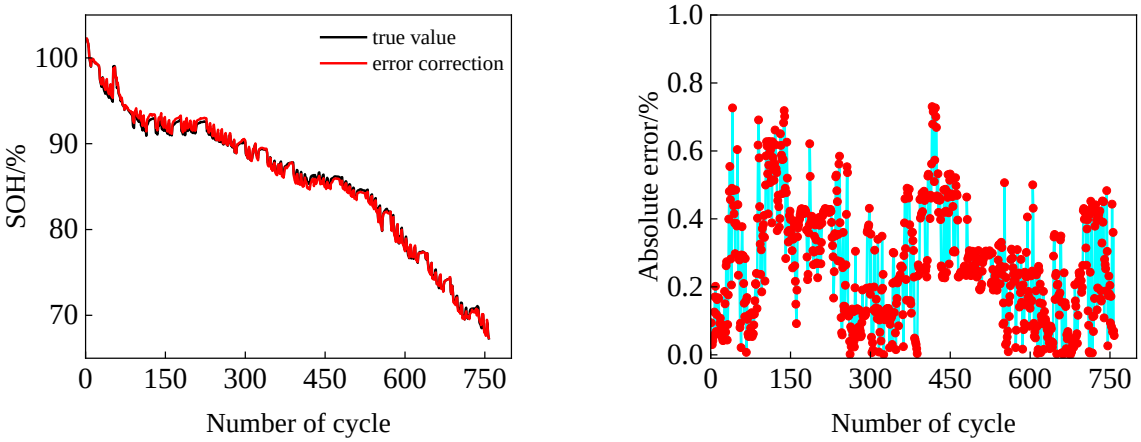

Figure 9. SOH estimation results and absolute errors of CS37 after error correction.

4.5. Validation on Other Datasets

To further verify the generalization ability of the proposed model, this section introduces experimental analyses using the Oxford Battery Aging Dataset and the NASA Battery Aging Dataset. Cell1 and Cell4 were selected as test samples from the Oxford dataset, while B0005 and B0007 were selected from the NASA dataset for validation.

Table 7 presents the SOH estimation errors on different datasets before and after error correction, where RMSE and MAE denote the root mean square error and mean absolute error before correction, respectively, while RMSE* and MAE* represent the errors after correction. As shown in the table, before error correction, the average RMSE and MAE of the CNN-GRU model on the Oxford dataset are 0.3603% and 0.2955%, respectively, while the corresponding values on the NASA dataset are 1.2190% and 1.0690%. After applying error correction, the average RMSE and MAE on the Oxford dataset decrease to 0.2234% and 0.1632%, respectively, while those on the NASA dataset decrease to 0.9075% and 0.7147%. The significant reduction in errors after correction demonstrates that

the proposed GPR-MC error correction strategy effectively optimizes the initial prediction results.

Figure 10 further illustrates the SOH estimation results on the Oxford and NASA datasets before and after error correction. It can be clearly observed that the corrected estimates better track the actual values, and the model's estimation accuracy is significantly improved.

Table 7. Estimation Errors Before and After Error Correction.

Battery	RMSE (%)	MAE (%)	RMSE* (%)	MAE* (%)
Cell1	0.3465	0.2868	0.1836	0.1292
Cell4	0.3741	0.3041	0.2631	0.1972
Average	0.3603	0.2955	0.2234	0.1632
B0005	1.2382	1.0845	0.8678	0.6336
B0007	1.1998	1.0535	0.9472	0.7957
Average	1.2190	1.0690	0.9075	0.7147

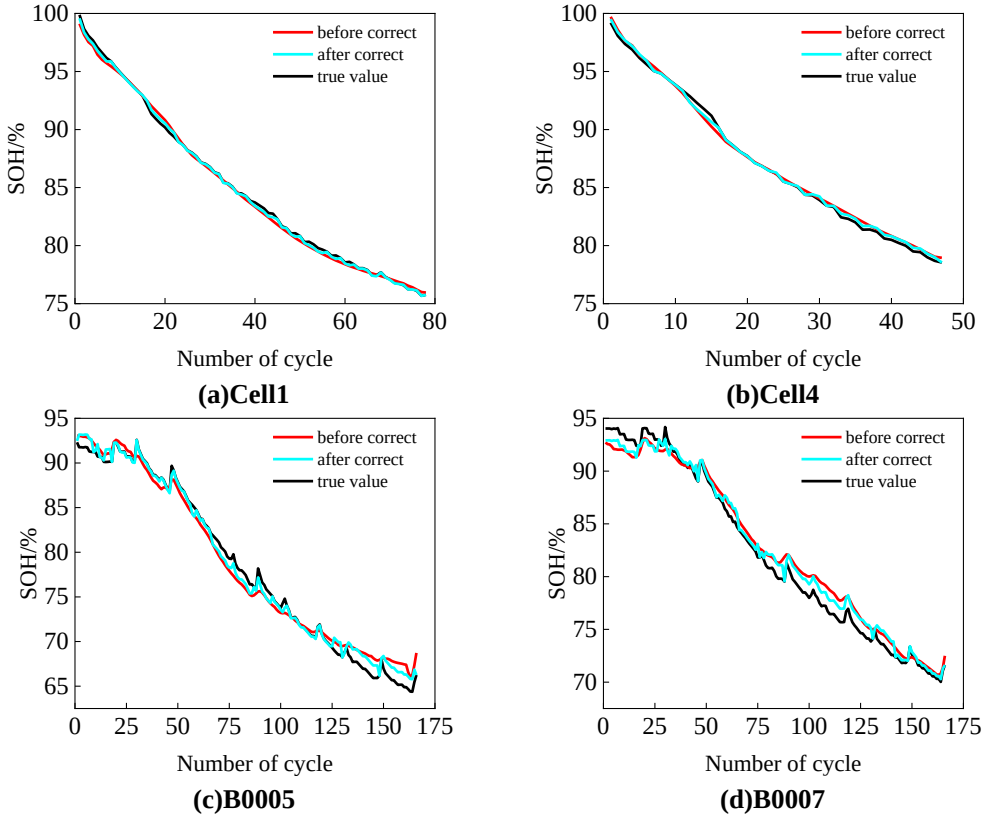

Figure 10. SOH Estimation Results Before and After Error Correction.

5. Conclusion

This study presents a novel method for estimating battery SOH using a CNN-GRU-based deep learning framework, augmented with a GPR-MC error correction strategy. The proposed approach has been thoroughly validated through experiments, demonstrating its effectiveness and distinct advantages. Firstly, the methodology derives health features from partial charging data, reducing the dependency on comprehensive datasets and thereby improving the model's adaptability and utility in practical, real-world scenarios. Secondly, the framework capitalizes on the CNN's robust feature extraction capabilities and the GRU's proficiency in processing sequential temporal data, enabling precise tracking of dynamic variations in the battery aging process and significantly enhancing SOH estimation accuracy. Moreover, to further refine the estimation results, the inclusion of the GPR-MC error correction strategy provides additional optimization to the initial SOH predictions. The experimental findings confirm that this strategy markedly enhances the model's prediction accuracy.

Acknowledgments

The authors gratefully acknowledge the support provided by the Shandong Province Science and Technology Program for Small and Medium-Sized Enterprise Innovation Capacity Enhancement [Grant Nos. 2023TSGC0173 and 2023TSGC0185]. Additional support

was received from the Shandong Province Undergraduate Teaching Reform Research Project, titled "Development of the 'Artificial Intelligence + X' Public Teaching Platform" [Grant No. M2020202].

References

1. Safavi V, Vaniar AM, Bazmohammadi N, et al. Battery Life Prediction Using Physics-Based Modeling and Coati Optimization. Energy Informatics,2025, 15272:303–313, https://doi.org/10.1007/978-3-031-74741-0_20
2. Gao MY, Shen HD, Bao ZY, et al. A Correlation-Augmented Informer-Based Method for State-of-Health Estimation of Li-Ion Batteries. IEEE Sensors Journal, 2024,24: 3342-3353, https://doi.org/10.1109/JSEN.2023.3341857
3. Bai JQ, Huang JY, Luo, K, et al. A feature reuse based multi-model fusion method for state of health estimation of lithium-ion batteries. Journal of Energy Storage,2023,70:107965, https://doi.org/10.1016/j.est.2023.107965
4. Safavi V, Vaniar AM, Bazmohammadi N, et al. Battery Remaining Useful Life Prediction Using Machine Learning Models: A Comparative Study. Information,2024,15:124, https://doi.org/10.3390/info15030124
5. Bustos R, Gadsden SA, Malysz P, et al. Health Monitoring of Lithium-Ion Batteries Using Dual Filters. Energies ,2022, 15:2230, https://doi.org/10.3390/en15062230
6. Ranga MR, Aduru VR, Krishna NV, et al. An Unscented Kalman Filter-Based Robust State of Health Prediction Technique for Lithium Ion Batteries. Batteries 2023, 9: 376, https://doi.org/10.3390/batteries9070376
7. Ling LY, Wei Y. State-of-Charge and State-of-Health Estimation for Lithium-Ion Batteries Based on Dual Fractional-Order Extended Kalman Filter and Online Parameter Identification. IEEE Access,2021,9: 47588-47602, https://doi.org/10.1109/ACCESS.2021.3068813
8. Xiong R, Wang S, Feng F, et al. Co-Estimation of State-of-Charge and State-of-Health for High-Capacity Lithium-Ion Batteries. Batteries 2023,9:509, https://doi.org/10.3390/batteries9100509
9. Chen BL, Liu YG, Xiao B. A novel hybrid neural network-based SOH and RUL estimation method for lithium-ion batteries. Journal of Energy Storage,2024, 98: 113074, https://doi.org/10.1016/j.est.2024.113074
10. Sui X, He S, Vilsen SB, et al. A review of non-probabilistic machine learning-based state of health estimation techniques for Lithium-ion battery. Applied Energy,2021, 300:117346, https://doi.org/10.1016/j.apenergy.2021.117346
11. Zhi Y, Wang HQ, Wang L. A state of health estimation method for electric vehicle Li-ion batteries using GA-PSO-SVR. Complex & Intelligent Systems ,2022,8:2167–2182, https://doi.org/10.1007/s40747-021-00639-9
12. Dai HD, Wang JX, Huang YY, et al. Lightweight state-of-health estimation of lithium-ion batteries based on statistical feature optimization. Renewable Energy,2024, 222:119907, https://doi.org/10.1016/j.renene.2023.119907
13. Wu C, Fu J, Huang X, et al. Lithium-Ion Battery Health State Prediction Based on VMD and DBO-SVR. Energies,2023,16: 3993, https://doi.org/10.3390/en16103993
14. Wu M, Yue C, Zhang F, et al. State of Health Estimation and Remaining Useful Life Prediction of Lithium-Ion Batteries by Charging Feature Extraction and Ridge Regression. Applied Sciences, 2024, 14: 3153, https://doi.org/10.3390/app14083153
15. Wang JW, Deng ZW, Yu T, et al. State of health estimation based on modified Gaussian process regression for lithium-ion batteries. Journal of Energy Storage,2022,51:104512, https://doi.org/10.1016/j.est.2022.104512
16. Vanem E, Salucci CB, Bakdi A, et al. Data-driven state of health modelling—A review of state of the art and reflections on applications for maritime battery systems. Journal of Energy Storage,2021,43:103158, https://doi.org/10.1016/j.est.2021.103158
17. Liao Y, Ma XC, Guo L, et al. State of health estimation for the lithium-ion batteries based on CNN-MLP network. Transactions of the Institute of Measurement and Control,2024:1–9, https://doi.org/10.1177/01423312241262947
18. Wang JX, Zhu LQ, Dai HD, et al. An efficient state-of-health estimation method for lithium-ion batteries based on feature-importance ranking strategy and PSO-GRNN algorithm. Journal of Energy Storage,2023,72:108638, https://doi.org/10.1016/j.est.2023.108638
19. Geng CM, Zhang TH, Chen B, et al. Battery State of Health estimation using GA-BP neural network on data feature mining. IEICE Electronics Express, 2023,20:1–5, https://doi.org/10.1587/elex.20.20230370
20. Xu HW, Wu LF, Xiong SZ, et al. An improved CNN-LSTM model-based state-of-health estimation approach for lithium-ion batteries. Energy,2023,276:127585, https://doi.org/10.1016/j.energy.2023.127585
21. Lin MQ, Wu J, Meng JH, et al. State of health estimation with attentional long short-term memory network for lithium-ion batteries.

Energy,2023,268:126706, https://doi.org/10.1016/j.energy.2023.126706

22. Park K, Choi Y, Choi WJ, et al. LSTM-Based Battery Remaining Useful Life Prediction With Multi-Channel Charging Profiles. IEEE Access,2020,8: 20786-20798, https://doi.org/10.1109/ACCESS.2020.2968939
23. Dai HD, Zhao GC, Lin MQ, et al. A novel estimation method for the state of health of lithium-ion battery using prior knowledge-based neural network and Markov chain. IEEE Transactions on Industrial Electronics,2019, 66: 7706-7716, https://doi.org/10.1109/TIE.2018.2880703
24. Ping F, Miao X, Yu H, et al. An Improved LSTNet Approach for State-of-Health Estimation of Automotive Lithium-Ion Battery. Electronics, 2023,12:2647, https://doi.org/10.3390/electronics12122647
25. Li R, Liu P, Li K, et al. AdaBoost.Rt-LSTM Based Joint SOC and SOH Estimation Method for Retired Batteries. Batteries, 2023, 9:425. https://doi.org/10.3390/batteries9080425
26. Wang XH, Dai K, Hu M, et al. Lithium-ion battery health state and remaining useful life prediction based on hybrid model MFE-GRU-TCA. Journal of Energy Storage,2024, 95:112442, https://doi.org/10.1016/j.est.2024.112442
27. Nasimov R, Kumar D, Rizwan M, et al. A Novel Approach for State of Health Estimation of Lithium-Ion Batteries Based on Improved PSO Neural Network Model. Processes, 2024, 12:1806, https://doi.org/10.3390/pr12091806
28. Li CR, Han XJ, Zhang Q, et al. State-of-health and remaining-useful-life estimations of lithium-ion battery based on temporal convolutional network-long short-term memory. Journal of Energy Storage,2023,74:109498, https://doi.org/10.1016/j.est.2023.109498
29. Song SX, Fei C, Xia HY, et al. Lithium-Ion Battery SOH Estimation Based on XGBoost Algorithm with Accuracy Correction. Energies, 2020, 13: 812, https://doi.org/10.3390/en13040812
30. Zhao GC, Lin MQ, D HD, et al. A Modified Strategy Using the KNN-Markov Chain for SOH Estimation of Lithium Batteries. Acta Automatic Sinica,2021,47:453-463, https://doi.org/10.16383/j.aas.c180124
31. Wei ZX, Han XJ, Li JR. State of health assessment for echelon utilization batteries based on deep neural network learning with error correction. Journal of Energy Storage,2022, 51:104428, https://doi.org/10.1016/j.est.2022.104428
32. Zou B, Xiong M, Wang H, et al. A Deep Learning Approach for State-of-Health Estimation of Lithium-Ion Batteries Based on a Multi-Feature and Attention Mechanism Collaboration. Batteries,2023, 9:329, https://doi.org/10.3390/batteries9060329
33. Qu JB, Wang YJ, Zheng RX, et al. A novel sequential estimation framework for battery state of health and remaining useful life based on sparse and limited data. Journal of Energy Storage,2024,99:113086, https://doi.org/10.1016/j.est.2024.113086
34. Safavi V, Vaniar AM, Bazmohammadi N, et al. Early prediction of battery remaining useful life using CNN-XGBoost model and Coati optimization algorithm. Journal of Energy Storage,2024,98 :113176, https://doi.org/10.1016/j.est.2024.113176

Data Availability Statement

CALCE Battery Dataset: https://calce.umd.edu/battery-data.

NASA Dataset: https://www.nasa.gov/intelligent-systems-division/

Oxford University Dataset: https://battery-intelligence-lab.github.io/

List of Abbreviations

SOH	State of Health	MC	Markov chain
BMS	Battery Management System	GPR	Gaussian Process Regression
CNN	Convolutional Neural Network	HF	Health Feature
GRU	Gated Recurrent Unit	RMSE	Root Mean Square Error
RNN	Recurrent Neural Network	MAE	Mean Absolute Error
KF	Kalman Filter	DTV	Differential Thermal Voltage
SIF	Sliding Innovation Filter	VMD	Variational Mode Decomposition
UKF	Unscented Kalman Filter	DBO	Dung Beetle Optimization
RUL	Remaining Useful Life	RR	Ridge Regression
GA	Genetic Algorithm	AM	Attention Mechanism
PSO	Particle Swarm Optimization	MLP	Multi-Layer Perceptron
SVR	Support Vector Regression	BP	Back Propagation
IC	Incremental Capacity	LSTM	Long Short-Term Memory

SOC	State of Charge	MFE	Multi-Feature Extraction
PKNN	Prior Knowledge Neural Network	DAEKF	Dual Adaptive Extended Kalman Filtering,
IPSO	Improved Particle Swarm Optimization	TCA	Temporal Convolutional Attention
BiLSTM	Bidirectional Long Short-Term Memory	TCN	Temporal Convolutional Network
GRNN	Generalized Regression Neural Network	DEKF	Dual Fractional-Order Extended Kalman Filter